Journal of Magnetic Resonance 207 (2010) 283–286

Contents lists available at ScienceDirect

Journal of Magnetic Resonance

journal homepage: www.elsevier.com/locate/jmr

Fitting of EPR spectra: The importance of a flexible bandwidth

Hasan Husein Mor, Høgni Weihe *, Jesper Bendix *

Department of Chemistry, University of Copenhagen, Universitetsparken 5, DK-2100 Copenhagen, Denmark

ARTICLE INFO

Article history:
Received 31 July 2009
Revised 16 September 2010

Keywords:
EPR
Fitting
Spin Hamiltonian
Bandwidth
Bandshape

ABSTRACT

Utilizing a standard spin Hamiltonian for an $S = \frac{3}{2}$ spin system, we fit complete X-band powder EPR spectra of the $Cr(oxalate)_3^{3-}$ anion diluted into $K_3[Co(oxalate)_3]\cdot 3H_2O$. By using models for the bandshape and bandwidths of varying degree of flexibility, we show that the successful outcome of such a fitting endeavour very much depends on the used bandshape–bandwidth model. The best results are obtained when the bandwidth model incorporates anisotropic intrinsic bandwidths in addition to being able to account for inhomogeneous line broadening caused by distributions of the spin Hamiltonian parameters.

1. Introduction

Spin Hamiltonian parameters for the tris-oxalatochromate(III) anion, $\left[Cr\ (ox)_3^{3-}\right]\left(ox = C_2O_4^{2-}\right)$, in various hosts have been determined on several occations; by EPR spectroscopy on single crystals [1,2,4], and also by sophisticated spectroscopy in the visible spectral region [3]. Previous investigations have determined values for the parameters D, E, g_x, g_y, and g_z of the spin Hamiltonian

$$\widehat{H} = D\left[\widehat{S}_z^2 - \frac{5}{4}\right] + E\left(\widehat{S}_x^2 - \widehat{S}_y^2\right) + \mu_B\left(g_x\widehat{S}_xB_x + g_y\widehat{S}_yB_y + g_z\widehat{S}_zB_z\right), \quad (1)$$

which is appropriate for an $S = \frac{3}{2}$ spin system. B_x, B_y, and B_z are the three components of the magnetic field vector. The spin Hamiltonian parameters were found to be only slightly depending on the host: $|D|$ values in the interval from 0.63 cm^{-1} to 0.7786 cm^{-1} have been reported, and according to [4] D is positive; E values in the interval 0.0–0.101 cm^{-1}, and, finally, reported g factors lie in the interval 1.963–1.982.

The purpose of this paper is *not* to redo previous investigations of the $Cr(ox)_3^{3-}$ anion. Rather we would like to pose two questions: Firstly, is it possible to extract the spin Hamiltonian parameters directly from a powder EPR spectrum by fitting a theoretical spectrum based on Eq. (1) to the full experimental spectrum and not to subjectively determined line positions; and, secondly, to which extent depends the outcome of such a fitting procedure on the applied bandshape/bandwidth model.

To the best of our knowledge, only a few authors have attempted to fit full EPR spectral traces, see Refs. [5–10]. These authors have all acknowledged that the very nature of a standard EPR spectrum – being a derivative spectrum – results in a multidimensional χ^2 surface having very complicated anatomy, filled with local minima and maxima. In a fitting situation this, unfortunately, implies that the initial guesses of model parameter values need to be essentially perfect in order to achieve convergence. As a result of this, Sojka [7] adapted the genetic algorithm to this particular problem. Although being able to localise the global minimum, this method suffers from needing an exorbitant number of iterations to locate the minimum. An elegant, and apparently overlooked, solution to the problems associated with derivative-based fittings has been put forward by Rakitin, see Chapter 3.2 in Ref. [11]. In short, this solution implies that in the initial stages of the analysis one fits the double-integrated spectrum, in a middle stage the absorption spectrum, and finally the derivative spectrum as recorded experimentally. We make use of this idea and typically need 5–10 iterations compared to >100,000 needed in Ref. [7].

This paper is organised as follows. After a short *Experimental* section we briefly discuss the all computed quantities in Section *Calculations*. Finally, we discuss the importance of the bandshape and bandwidth on a successful outcome of an spectral analysis based on least-squares fitting.

2. Experimental

Potassium tris-oxalatochromate trihydrate and the analogous cobalt salt were synthesised according to Ref. [13]. Crystals of the cobalt salt containing small amounts of $Cr(ox)_3^{3-}$ were grown from solutions containing 0.1% of the chromium salt. EPR spectra were recorded at $T = 70$ K on a Bruker Elexsys spectrometer operating at X-band frequencies.

* Corresponding authors.
E-mail addresses: weihe@kiku.dk (H. Weihe), bendix@kiku.dk (J. Bendix).

1090-7807/$ - see front matter © 2010 Elsevier Inc. All rights reserved.
doi:10.1016/j.jmr.2010.09.011

3. Calculations

For each field value and for each orientation of the magnetic field we compute the contribution y from an energy level pair (a,b) to the absorption spectrum as

$$y_{ab} = P \times (p_a - p_b) \times V(\Delta_{ab}, h\nu, \Gamma_{ab}), \tag{2}$$

where p_a and p_b is the thermal population of energy level a and b, respectively.

$$p_a = \frac{\exp(\lambda_a/k_B T)}{\sum_i \exp(\lambda_i/k_B T)}, \tag{3}$$

with λ_a, k_B, and T being the ath eigenvalue, Boltzmann constant, and the absolute temperature, respectively. Here, the eigenvalues and the corresponding eigenvectors needed for computation of the intensity, see Eq. (4), are obtained by a numerical diagonalisation of the matrix representation of the spin Hamiltonian of Eq. (1).

P is the transition probability

$$P \propto |\langle \boldsymbol{u}_b | \boldsymbol{\mu}_{mw} \cdot \hat{\boldsymbol{\mu}} | \boldsymbol{u}_a \rangle|^2 \tag{4}$$

Here, $\boldsymbol{u}_a$ is the ath eigenvector corresponding to the eigenvalue λ_a; $\boldsymbol{\mu}_{mw}$ is the time-independent part of the magnetic component of the microwave radiation, and $\hat{\boldsymbol{\mu}}$ is the magnetic moment vector operator of the spin system, $\hat{\boldsymbol{\mu}} = \left(\partial\hat{H}/\partial B_x, \partial\hat{H}/\partial B_y, \partial\hat{H}/\partial B_z\right)$.

The last symbol introduced in Eq. (2), V, is a bandshape function expressed in energy variables. In order to introduce some flexibility in the bandshape, we use here a naive but popular approximation of the Voigt profile which is a linear combination of a Lorentzian and a Gaussian as a bandshape [12]

$$V(\Delta_{ab}, h\nu, \Gamma_{ab}) = \upsilon L(\Delta_{ab}, h\nu, \Gamma_{ab}) + (1-\upsilon) G(\Delta_{ab}, h\nu, \Gamma_{ab}). \tag{5}$$

Δ_{ab} is the energy difference between energy level b and a, $\Delta_{ab} = \lambda_b - \lambda_a$; $h\nu$ is the energy equivalent of the microwave radiation, and Γ_{ab} is the bandwidth to be used for this particular pair of energy levels. Here, we assume that all pairs a, b are associated with the same bandshape, i.e. the same value of the parameter υ. In this work we use the following form for Γ_{ab}

$$\Gamma_{ab}^2 = l_x^2\Gamma_x^2 + l_y^2\Gamma_y^2 + l_z^2\Gamma_z^2 + \sum_p \left(\frac{\partial \Delta_{ab}}{\partial p}\right)^2 \sigma_p^2, \tag{6}$$

where p is a parameter of the spin Hamiltonian. The three symbols Γ_x, Γ_y, and Γ_z are the three components of an orientation-dependent bandwidth and the l factors are direction cosines. In this work we have assumed Γ_x being the same for all a, b pairs and similarly with Γ_y and Γ_z. The last term of Eq. (6) accounts for the contribution to the bandwidth caused by distributions of the spin Hamiltonian parameters; accordingly, transitions will have different bandwidths depending on the levels involved and their energetic sensitivity $(\partial\Delta_{ab}/\partial p)$ towards the spin Hamiltonian parameters.

The powder spectrum is obtained by summing Eq. (2) for 600 values of the polar angle between 0° and 90° and for 200 values of the azimutal angle between 0° and 90°.

As mentioned in the introduction, we initially fit the double-integrated spectrum and then the absorption spectrum. Finally, we minimise

$$\chi^2 = \sum_i \left(\frac{y_{o,i} - y_{c,i}}{\sigma_i}\right)^2. \tag{7}$$

Here, $y_{o,i}$ and $y_{c,i}$ is the ith observed and calculated data point, respectively, σ_i is the error on the ith data point, and the summation runs over all the points in the spectrum. The details of the implementation of the ideas put forward in Ref. [11] will be the subject of a forthcoming publication. See refs [14,15] for some successful applications of the method.

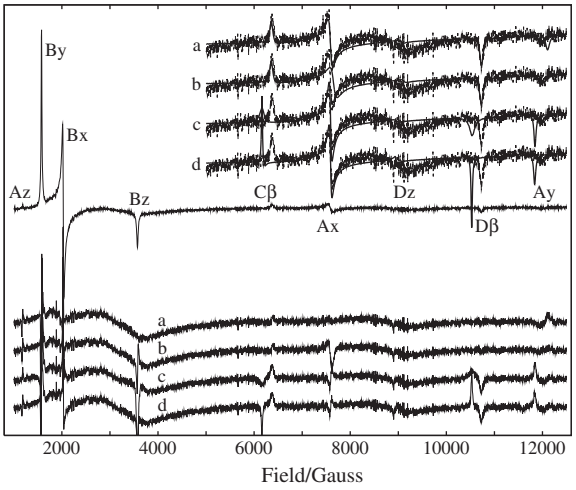

Fig. 1. EPR spectra of $Cr(ox)_3^{3-}$ in powdered $K_3[Co(ox)_3]\cdot 3H_2O$. The middle trace is the experimental spectrum. The visible features in the spectrum are designated by symbols defined in Fig. 2. The four lower traces are the differences between the experimental and the calculated spectra. The four upper traces show the high-field portion of the experimental and the fitted spectra magnified by a factor of 10. The labels "a", "b", "c", and "d" designate the four models used to fit the spectra.

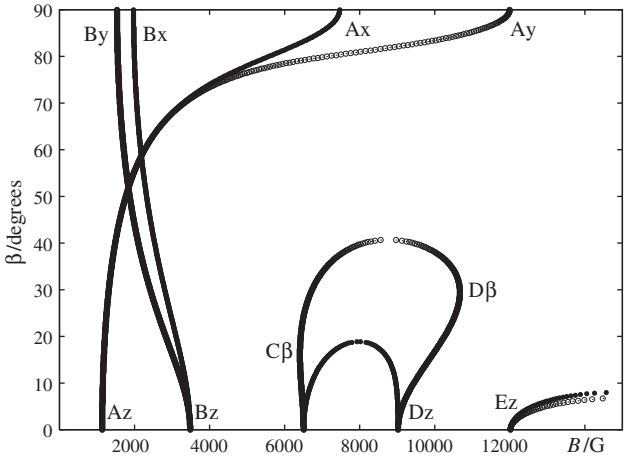

Fig. 2. Angular dependencies of the resonance magnetic fields in the zx (filled circles) and the zy (open circles) plane. The labels designate angular regions giving rise to visible features in the powder spectrum of Fig. 1.

4. Results and discussion

The experimental derivative spectrum, as recorded, is shown in Fig. 1. The visible features in the spectrum have been designated by symbols defined in Fig. 2. The absorption-like features Az, By, Bz, Cβ, Dβ, and Ay exhibit clearly different linewidths in the range from 14 to 130 Gauss measured as the full width at half height. Similarly, the derivative-like features Bx and Ax exhibit peak-to-peak widths of 25 and 80 Gauss, respectively. This order-of-magnitude variation in linewidths clearly suggests that a line broadening mechanism must be included in the model if a quantitative reproduction of the spectrum is to be expected.

The linewidths of features Az and Bz are approximately 14 and 40 Gauss, respectively. Both features originate from transitions corresponding to the magnetic field being parallel, or nearly so,

to the molecular z axis; Az from the transition $|\frac{-3}{2}\rangle$ to $|\frac{3}{2}\rangle$, and Bz from the transition $|\frac{-1}{2}\rangle$ to $|\frac{1}{2}\rangle$. The ratio of these two bandwidths is close to 3 in field units, as expected [16] if the transitions had the same bandwidth in energy units. Therefore, the validity of the assumption is supported that all transitions are assigned the same un-broadened width, see Eq. (6) and the text thereafter.

As evident in the spectrum of Fig. 1, the features above 4000G are much weaker compared to the features in the low-field part of the spectrum. Hence, in a fitting context, the low-intensity part of the spectrum has a but minor contribution to the χ^2. Consequently, those parameters which are mainly determined by the low-intensity lines will obtain large standard deviations. To compensate, we set the σ_i-s for the high-field points to one fifth of the σ_i-s in the low-field part in order to give the high-field points additional weight in the fitting routine. By this, the two regions of the spectrum become comparable in terms of the ratio | intensity|/σ.

We have applied several different parametric models to the experimental spectrum. In the following these models are designated "a", "b", "c", and "d". The models differ by different numbers of parameters, as well as the number of model parameters optimised in the fitting routine. We have chosen to show the results of four of these models, see Table 1. These models represent cases with different number of spin Hamiltonian parameters and the same linewidth model, as well as the same spin Hamiltonian but different linewidth models.

All of the employed parametric models result in values of spin Hamiltonian parameters which are consistent with the earlier findings, see values quoted after Eq. (1). The non-zero E parameter reflects the fact that the anion in the host, $K_3[Co(ox)_3]\cdot 3H_2O$, is not located on a crystallographic site with three-fold symmetry. The range of g values in Table 1 is justified on the basis of simple ligand-field theory [17]. At an initial stage of the analysis we allowed for the pseudo Voigt lineshape, Eq. (5). However, for all models the parameter v optimised to values between 0.99(3) and 1.00(3) corresponding to an almost pure Lorentzian lineshape. Accordingly, we have left out this parameter from Table 1. The pure Lorentzian lineshape might be a result of not including the 9.25% abundance of ^{53}Cr in the treatment. Unresolved hyperfine interactions to this nucleus adds a small intensity to the wings of all EPR lines resulting in an approximate Lorentzian lineshape. The fact that the *bandshape* in our, admittedly naive, bandshape model, Eq. (5), could be represented by the same value of the parameter v, allows us to discuss the effect of the *bandwidth* alone.

First, model "a" and model "b" are compared. These two models are defined by having the same bandwidth but different spin Hamiltonian operators. In model "a" we allow g_x to be different from g_y which in principle is allowed in the absence of strict trigonal symmetry, whereas in model "b" we fixed g_x to g_y. From the traces designated "a" in Fig. 1 it can be seen that model "a" reproduces line positions as well as line widths very well. The broad feature between 8000 and 10,000 Gauss cannot be reproduced by any of the applied models. The main change seen in the residual when g_x is fixed to g_y is located around the features Ax, Ay, and Bz, compare upper traces "a" and "b" in Fig. 1. The field position of feature Ax and Ay is reproduced significantly worse and slightly better, respectively. The concomitant increase in χ^2 on going from model "a" to model "b" is large enough that on purely statistical grounds model "a" has to be favoured. Performing a standard statistical F-test [18] on χ^2_a and χ^2_b with their respective degrees of freedom the rather low probability of 8×10^{-14} is obtained that these two variances (χ^2-s) are drawn from the same distribution leading to the conclusion that model "a" is significantly better than model "b".

In model "c" the parameters σ_D and σ_E are omitted from the linewidth description, but the anisotropy w_x, $w_y \neq w_z$ is still allowed. If the g_z parameter were allowed to optimise freely, it arrived at a rather un-physical value below 1.93. Therefore it was fixed, see Table 1. The part of the linewidth accounted for by the broadening parameters σ_D and σ_E in the previous models is now absorbed by the linewidth parameters $w_x = w_y$ and w_z. Traces "c" of Fig. 1 display a large qualitative difference between the experimental and the computed spectrum; especially in the vicinity of the features Cβ, Dβ, and Ay, for which line positions are poorly reproduced. The increase in χ^2 is also significant as judged by an F-test, which yields a probability of 2×10^{-13} that the χ^2-s from model "b" and "c" are drawn from the same population. Phrased differently: model "b" is a significantly better model than "c". A comparison of trace "c", Fig. 1, with traces "b" and "a" shows that model "c" does not reproduce the line positions as well as the models "a" and "b".

Model "d" represents a further restriction in the flexibility of the bandwidth model. Here, all parameters w_x, w_y, and w_z are simply set equal resulting in a significant increase of χ^2. Inspection of traces "c" and "d", Fig. 1, shows that line positions in both models are poorly reproduced, and that the linewidths of "d" are poorer than those of "c".

In summary, it has been shown that attention should be given to the linewidth-lineshape model when fitting full EPR spectral traces. The present EPR spectrum of Cr^{3+} in powdered $K_3[Co(ox)_3]\cdot 3H_2O$, clearly illustrates that field positions of experimental spectral features are badly reproduced if the bandwidth model is not flexible enough to account for inhomogeneous line broadening. An un-flexible bandwidth model results in prominent features being reproduced on the expense of less prominent features.

Table 1
Model parameters as obtained from the fitting procedures. A horizontal line indicates that this parameter was not included. The number in parentheses is the estimated standard deviation on the last digit. The g_z parameter in model "c" was fixed; for an explanation see text. In all models there were two additional parameters accounting for a straight line background. The data points were weighted identically in the four models making the χ^2-s directly comparable. The overall scaling of the σ-s was chosen to make model "b" a statistically good model, i.e. with χ^2 equal to the degrees of freedom ($N_{data} - N_{fit}$).

	Model a	Model b	Model c	Model d
D/cm^{-1}	0.7178(2)	0.7171(3)	0.7008(2)	0.7010(1)
$E/10^{-4}$ cm^{-1}	606.7(4)	594.1(4)	580.0(2)	579.5(2)
g_x	1.9777(2)	$=g_y$	$=g_y$	$=g_y$
g_y	1.9656(2)	1.9711(1)	1.9706(2)	1.9717(1)
g_z	1.9806(5)	1.9744(7)	1.975*	1.9770(4)
$w_x = w_y/10^{-4}$ cm^{-1}	18.9(4)	15.6(6)	20.5(4)	20.4(4)
$w_z/10^{-4}$ cm^{-1}	15(1)	16(1)	99(6)	$=w_y$
$\sigma_D/10^{-4}$ cm^{-1}	35(2)	32(3)	–	–
$\sigma_E/10^{-4}$ cm^{-1}	9.8(8)	21(1)	–	–
χ^2	2386	3130	4090	5094

References

[1] Y. Kawasaki, L.S. Forster, Zero-field splittings in tris(oxalato-chromium)(III) complexes, J. Chem. Phys. 50 (2) (1969) 1010–1013.
[2] R.A. Bernheim, E.F. Reichenbecher, EPR of Cr(III) in a single crystal of $NaMgAl(C_2O_4)\cdot 9H_2O$, J. Chem. Phys. 51 (3) (1969) 996–1001.
[3] A. Hauser, H. Riesen, R. Pellaux, S. Decurtins, Resonant excitation energy transfer in $[Rh(bpy)_3][NaCr(ox)_3]ClO_4$, Chem. Phys. Lett. 261 (1996) 313–317.
[4] N. Novosel, D. Zilic, D. Pajic, M. Juric, B. Peric, K. Zadro, B. Rakvin, P. Planinic, EPR studies on single crystals of a heterometallic (Cu^{II} and Cr^{III}) complex: zero-field splitting determination, Solid State Sci. 10 (2008) 1387–1397.
[5] B. Kirste, Methods for automated analysis and simulation of electron paramagnetic resonance spectra, Anal. Chim. Acta 256 (1992) 191–200.
[6] S.K. Misra, A rigorous evaluation of spin-Hamiltonian parameters and linewidth from a polycrystalline EPR spectrum, J. Magn. Reson. 140 (1999) 179–188.
[7] T. Spalek, P. Pietrzyk, Z. Sojka, Application of the genetic algorithm joint with the Powell method to nonlinear least-squares fitting of powder EPR spectra, J. Chem. Inf. Model. 45 (2005) 18–29.

[8] A. Lund, H. Gustafsson, J. Maruani, M. Shiotani, Automatic fitting to powder EPR spectra of coupled paramagnetic species employing Feynman's theorem, Spectrochim. Acta A63 (2006) 830–835.
[9] S. Stoll, A. Schweiger, EasySpin, a comprehensive software package for spectral simulation and analysis in EPR, J. Magn. Reson. 178 (2006) 42–55 (Later versions of this software package include the option of fitting spectra).
[10] G.R. Hanson, K.E. Gates, C.J. Noble, M. Griffin, A. Mitchell, S. Benson, XSophe-Sophe-XeprView. A computer simulation software suite (v.1.1.3) for the analysis of continuous wave EPR spectra, J. Inorg. Biochem. 98 (2004) 903–916.
[11] Yu.V. Rakitin, G.M. Larin, V.V. Minin, Interpretation of ESR spectra of coordination compounds, Nauka, 1993. ISBN 5-02-001570-9.
[12] S.D. Bruce, J. Higinbotham, I. Marshall, P.B. Beswick, An analytical derivation of a popular approximation of the Voigt function for quantification of NMR spectra, J. Magn. Reson. 142 (2000) 57–63.
[13] J.C. Bailar Jr., E.M. Jones, Trioxalato salts, Inorg. Synth. 1 (1939) 35–38.
[14] C.A. Thuesen, A.-L. Barra, J. Glerup, Single crystal electron paramagnetic resonance spectra of Cs_2MnF_6 and K_2MnF_6 diluted in the isomorphous germanium salts, Inorg. Chem. 48 (2009) 3198–3204.
[15] S. Piligkos, I. Laursen, A. Morgenstjerne, H. Weihe, Sign and magnitude of spin Hamiltonian parameters for Mn^{2+} impurities in calcite. A multi- and low-frequency EPR study, Mol. Phys. 105 (15) (2007) 2025–2030.
[16] J.R. Pilbrow, Transition Ion Electron Paramagnetic Resonance, Clarendon Press, Oxford, 1990.
[17] J.S. Griffith, The Theory of Transition Metal Ions, Cambridge University Press, 1961.
[18] D.G. Kleinbaum, L.L. Cupper, K.E. Muller, A. Nizam, Applied Regression Analysis and Other Multivariable Methods, Duxbury Press, New York, 1997. pp. 426–434.